JOURNAL OF GEOPHYSICAL RESEARCH, VOL. 104, NO. B7, PAGES 15,025–15,041, JULY 10, 1999

Lithospheric deformation beneath the San Gabriel Mountains in the southern California Transverse Ranges

Monica D. Kohler

Department of Earth and Space Sciences, University of California, Los Angeles

Abstract. High-resolution tomographic images from Los Angeles Region Seismic Experiment (LARSE) array and southern California Seismic Network (SCSN) teleseismic data suggest that the entire lithosphere below the San Gabriel Mountains and San Andreas fault in the Transverse Ranges has thickened in a narrow, vertical sheet. *P* wave travel time inversions of the combined data support the presence of the well-documented upper mantle high-velocity anomaly that extends ~200 km into the mantle under the northernmost Los Angeles basin and Transverse Ranges, and is associated with mantle downwelling due to oblique convergence. We find that the high-velocity, high-density upper mantle anomaly comprises a 60-80 km wide sheet of mantle material that lies directly below a substantial crustal root in the San Gabriel Mountains. The velocity perturbations are as large as 3% in the anomaly, corresponding to a ~2% density increase. The tomographic images suggest that deformation in the ductile lower crust and mantle lithosphere may be partially coupled mechanically and thermally if the thickening is occurring together in response to convergence and that it may be a local compressional feature.

1. Introduction

The Transverse Ranges in southern California are the result of recent, diffuse transpressional plate boundary tectonics in which the strike-slip San Andreas fault and a network of smaller strike-slip and thrust faults producing the Transverse Ranges define the oblique motion plate boundary between the Pacific and North American plates (Figure 1). Lithosphere at the plate boundary has been subjected to major episodes of extension and convergence that have left their mark on surface and subsurface deformation. The goal of this paper is to illustrate the kinematic relationship between the crust and uppermost mantle by tomographic imaging of southern California lithosphere at the plate boundary. New, tight constraints are provided by a combined data set that includes high-density Los Angeles Region Seismic Experiment (LARSE) array and Southern California Seismic Network (SCSN) teleseismic data. This study builds on previous work that showed significant crustal thickness variations in a two-dimensional slice across the San Gabriel Mountains and San Andreas fault [*Kohler and Davis*, 1997].

The convergence of the East Pacific Rise with the western boundary of the North American plate marked the end of Farallon plate subduction 37-30 Myr ago [*Atwater*, 1970; *Engebretson et al.*, 1985] (see *Wright* [1991] for a review of southern California tectonic history). The Los Angeles region and Mojave Desert subsequently underwent crustal extension and rifting that began 24-18 Myr ago [*Dokka*, 1989; *Tennyson*, 1989; *Wright*, 1991], accommodated by transform motion on onshore strike-slip faults [*Stock and Hodges*, 1989; *Humphreys and Weldon*, 1994]. The Los Angeles basin probably developed as a local rift basin within the extensional environment and began to assume its present-day shape ~7 Myr ago when continued extension produced stretched, thinned crust and subsidence [*Yerkes et al.*, 1965; *Yeats*, 1978; *Wright*, 1991]. Uplift of the Transverse Ranges by north-south compression began ~5 Myr ago [*Crowell*, 1968; *Atwater*, 1970; *Wright*, 1991]. The Los Angeles basin and Transverse Ranges are now experiencing contraction distributed over a broad network of blind thrust, strike-slip, and oblique-slip faults [*Feigl et al.*, 1993; *Shen et al.*, 1996, 1997; *Walls et al.*, 1998].

Plate motion in southern California is approximately parallel to the San Andreas fault except where a segment of the fault in the Transverse Ranges takes a left step and is oriented more east-west, corresponding to a region that has experienced recent compression [*Feigl et al.*, 1993]. The formation of the left step in the San Andreas fault occurred 12-4 Myr ago [*Crowell*, 1968; *Atwater*, 1970; *Stock and Hodges*, 1989; *Wright*, 1991] and is the most likely source of oblique convergence in southern California [*Crowell*, 1968]. Tomography studies exhibit a high-velocity anomaly in the upper mantle below the Transverse Ranges [*Hadley and Kanamori*, 1977; *Raikes*, 1980; *Walck and Minster*, 1982; *Humphreys et al.*, 1984; *Humphreys and Clayton*, 1990; *Zhao et al.*, 1996] thought to be caused by mantle downwelling associated with the oblique convergent tectonics [*Bird and Rosenstock*, 1984; *Humphreys and Hager*, 1990]. The convergence is thought to be accommodated by translation and rotation of crust, beneath which entirely decoupled mantle deformation is taking place [*Hadley and Kanamori*, 1977; *Bird and Rosenstock*, 1984;

Paper number 1999JB900141.
0148-0227/99/1999JB900141$09.00

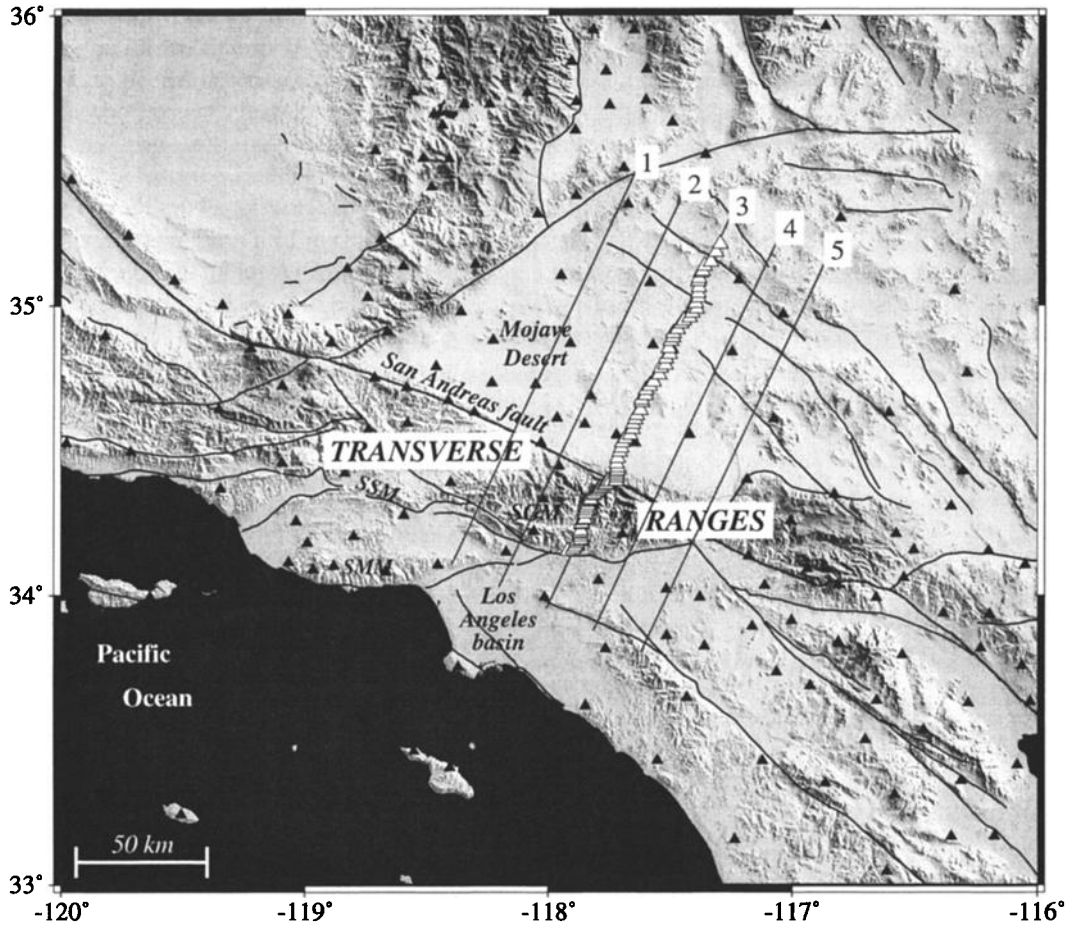

Figure 1. Shaded relief and fault map of southern California showing locations of Los Angeles Region Seismic Experiment (LARSE) passive array stations (open triangles) and Southern California Seismic Network stations (solid triangles). SMM, Santa Monica Mountains; SGM, San Gabriel Mountains; and SSM, Santa Susana Mountains. Regions for which two-dimensional cross sections will be shown are numbered as slices 1-5.

Humphreys and Clayton, 1990; *Humphreys and Weldon*, 1994].

Assumptions about the detailed geometry of the Moho beneath the San Gabriel Mountains have had a significant influence on interpretations of plate boundary dynamics. *Hadley and Kanamori* [1977] proposed the existence of a horizontal decoupling shear zone near an undeformed, flat Moho along which crustal motions diverge from the mantle. Their model of decoupled, differential motions between the crust and mantle implied that the lower crust was subject to shear but not to compression. *Bird and Rosenstock* [1984] used plate motion estimates and the tomographic images of *Raikes* [1980] to propose slablike lithospheric downwelling to accommodate a large amount of plate shortening. Their qualitative model suggested that the Moho may be depressed at the downwelling hinges because of the weight of the subducted mantle. *Humphreys and Hager* [1990] quantitatively modeled mantle flow to propose that relatively cold subcrustal lithosphere, decoupled from the uniformly thin crust above, is symmetrically descending into the mantle from both sides of the Transverse Ranges. They also invoked a decoupling zone near the Moho to explain why the crust would have uniform thickness in a region subject to compression.

Early lower crustal and upper mantle tomographic images use data from the Southern California Seismic Network, which, a decade ago, had an average station spacing of 20-30 km and larger in the Transverse Ranges. We show that the combination of more recently obtained teleseismic travel times from the LARSE array and those from the SCSN reveals shallow (<60 km), short-wavelength (<30 km) lithospheric heterogeneity not seen in studies based on sparser network data. In particular, results described in an earlier paper [*Kohler and Davis*, 1997] suggest that lateral crustal thickness variations do exist beneath the San Gabriel Mountains. Inversions of combined LARSE and network data for uppermost mantle structure, described in this paper, provide new information about the relationship between deformation in the lower crust and that in the uppermost mantle, which needs to be considered in models of upper mantle flow.

2. Teleseismic Travel Time Inversion

We combined teleseismic *P* wave travel time residuals from the very dense LARSE array with SCSN residuals to map three-dimensional lateral velocity variations in the upper mantle. To date, LARSE has consisted of a passive phase

(fall 1993) and an active phase (fall 1994). The LARSE passive phase took place between November 11, 1993, and December 16, 1993, and involved the installation of 88 short-period, three-component, digital seismometers along a linear southwest-northeast array in southern California (Figure 1, open triangles). The southern foothills of the San Gabriel Mountains were chosen as the starting point of the high-density array because they mark the transition from the high noise of the Los Angeles basin to the low noise of the San Gabriel Mountains and Mojave Desert. The first few stations were in the San Gabriel River fan (in the northernmost San Gabriel Valley) and in the San Gabriel Canyon (in the southern foothills of the San Gabriel Mountains). The average spacing between the stations was ~1 km in the San Gabriel Mountains and ~2 km in the Mojave Desert.

During the four weeks of recording, stations recorded continuous waveform data from several hundred teleseismic, regional, and local events. About 20 teleseisms had *P* wave arrivals from which travel times could be determined. These events fell into several distinct back azimuth groups, and the epicentral distances between sources and receivers ranged from 30°-90°. The earthquakes were located in the Aleutian Islands, Kamchatka, the Kuril Islands, the Mid-Atlantic Ridge, the Solomon Islands, Japan, the Fiji Islands, and Chile. Relative *P* wave travel times were measured with interactive computer software that determined the time corresponding to the maximum amplitude of the first visible upswing or downswing. Waveform coherence was high across the array. We determined 1161 teleseismic travel times from the LARSE array data. (See *Kohler et al.* [1996] and *Kohler and Davis* [1997] for a description of waveform characteristics, travel time residuals, and experiment details.)

The 1161 LARSE teleseismic residuals were combined with 2679 residuals obtained from SCSN stations (Figure 1, solid triangles). The SCSN data consist of handpicked teleseismic *P* wave travel time residuals compiled for several western United States tomography studies [*Raikes*, 1980; *Humphreys et al.*, 1984; *Humphreys and Clayton*, 1990; *Humphreys and Dueker*, 1994]. Our goal is to improve the resolution of the tomographic images in regions of maximum compression near the plate boundary.

We have the unique advantage over most other upper mantle studies that several high-resolution crustal velocity models are available to remove the effects of upper crustal heterogeneity. Arrivals that were recorded at LARSE stations were corrected for topography and crustal velocity variations by projecting the rays through the recent upper crustal velocity model of *Lutter et al.* [1999] to the elevation of each station. This model was obtained from the dense reflection-refraction profile along the same line during LARSE and represents the detailed velocity structure in the upper 10 km of the crust. The upper crustal velocity corrections applied to our teleseismic residuals functioned both as topography corrections and as station corrections. SCSN residuals had already been determined relative to a one-dimensional Earth model and were corrected for topography (using a *P* wave velocity of 5.5 km/s). The SCSN residuals (most of which were recorded >10 km from the LARSE array) were projected through the local, three-dimensional, upper crustal model of *Hauksson and Haase* [1997] to remove the uppermost 10 km of heterogeneity, since the model of *Lutter et al.* [1999] is only valid directly below the LARSE array. In the region where the crustal models overlap, the velocities from *Lutter et al.* [1999] exhibit features on a smaller scale, with finer resolution made possible by the dense array of explosion sources and receivers.

Next, we corrected the travel time residuals for variations in crustal thickness using the Moho depth variation model of *Kohler and Davis* [1997]. This model was obtained by inverting the same LARSE teleseismic *P* wave travel time residuals for Moho depth variations while assuming a simple, regional, three-dimensional block representation of the high-velocity mantle anomaly derived by *Humphreys and Clayton* [1990] and a constant lower crustal velocity. The model suggests a 12 km increase in crustal thickness from 28 km beneath the eastern edge of the Los Angeles basin to a 40 km thick crust beneath the San Gabriel Mountains. The anomalously deep Moho geometry is supported by the high-resolution LARSE active source imaging results. Reflectors appearing in the two-dimensional reflection-refraction profile along the same line suggest that the Moho dips beneath the San Gabriel Mountains on both sides, extending from 30 km to a maximum depth of 38 km beneath the San Andreas fault [*Fuis*, 1998; *Ryberg and Fuis*, 1998], and perhaps to a depth of >40 km as suggested by *PmP* arrivals [*Hafner et al.*, 1996].

Kohler and Davis [1997] also found evidence that the teleseismic *P* wave travel time data were sensitive to upper mantle structure. When they included a simple block representation of the upper mantle high-velocity anomaly [*Humphreys and Clayton*, 1990] in their inversions, the variance reduction from the fit to the residual data increased from 54% to 72%. Their results showed that even though most of the small-scale features in the signal could be described by variations in crustal thickness, upper mantle structure was also necessary to fit the residuals. The remaining residual travel times are used in the lithospheric tomographic inversions presented here and constrain velocity variations primarily in the upper 70 km of the resulting images.

The model space is parameterized as a three-dimensional grid with rows parallel to the LARSE array so that we could analyze lithospheric images in a slice beneath the array where the upper crust is known with the best resolution. The grid space corresponding to the final solution consists of 8580 boxes (i.e., parameters), each with dimensions of 10 km parallel to the array by 20 km perpendicular to the array by 10 km depth. Total grid space dimensions are 220 km parallel to the array by 300 km perpendicular to the array by 260 km depth. The network stations were limited to those <70 km from the LARSE array, but the grid is wider to allow for nonvertical ray projection. This parameterization represents a reasonable choice based on the resolution and root-mean-square (RMS) travel time fit trade-off. Ray path coverage within the boxes is best near the LARSE array but remains relatively uniform at most depths and distances from the array (Figure 2). Final tomographic images are contoured by linearly interpolating between the centers of each box. The ve-

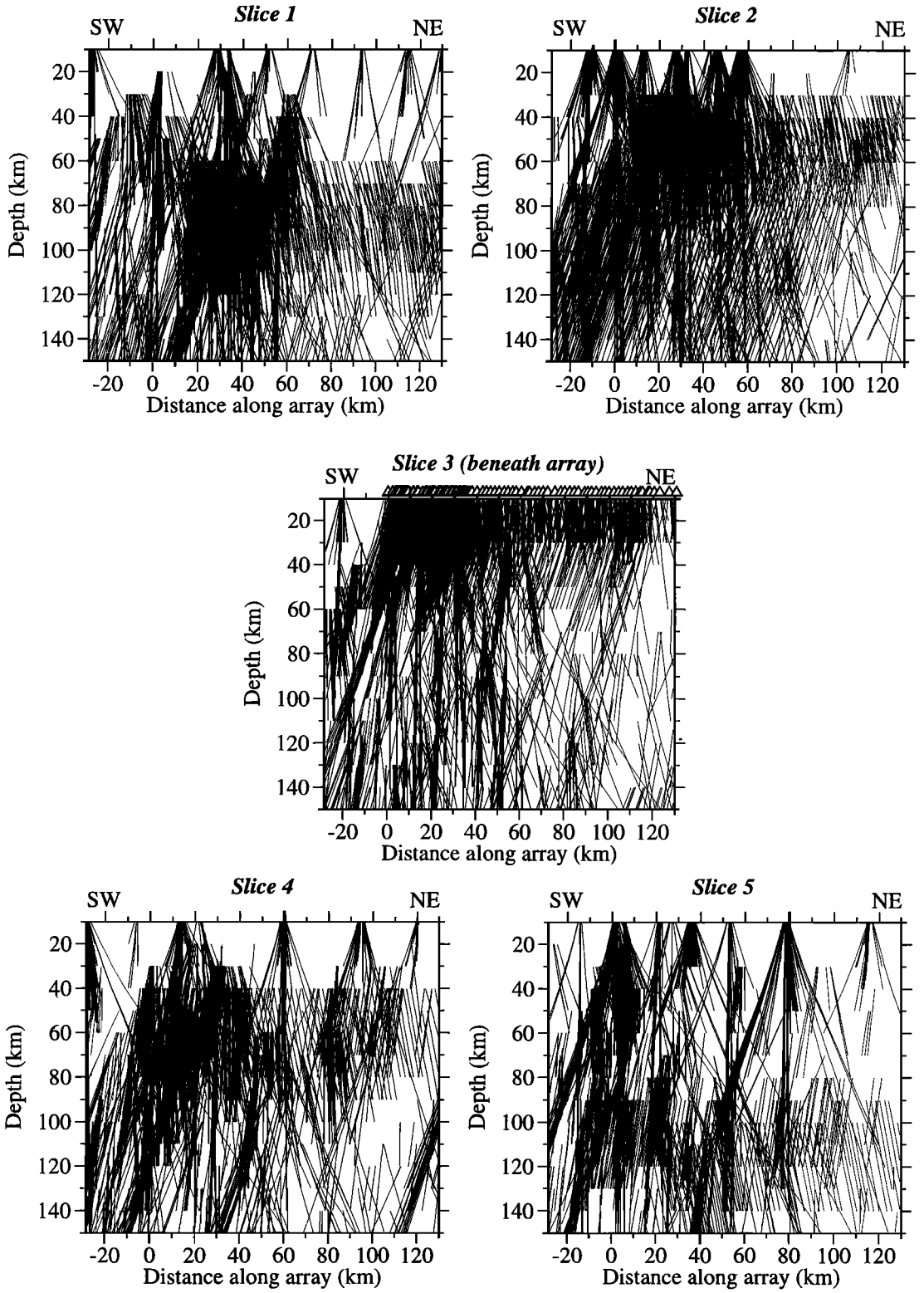

Figure 2. Ray path coverage in slices parallel to array. Rays appear truncated because they are entering the plane containing slice at an angle. See Figure 1 for locations corresponding to slice numbers.

locity perturbations were constrained to be zero in the uppermost 10 km of the model space for regions in which the upper crustal velocity corrections were made. This constraint applied to all residuals except those recorded at the far endpoints of the model space. We solved for velocity up to the surface for the few stations that lay outside both crustal model spaces (neither of which are as large as our grid space). The starting model, shown in Table 1, is based on the refraction velocities found by *Lutter et al.* [1999], the one-dimensional crustal model of *Hadley and Kanamori* [1977], and iasp91

Table 1. One-Dimensional Starting Velocity Model.

Depth Range, km	*P* Wave Velocity, km/s
0-10	5.5
10-30	6.5
30-90	7.8
90-100	8.0
100-200	8.1
200-220	8.2
220-240	8.3
240-260	8.4

Layers are parameterized in 10 km intervals.

[*Kennett and Engdahl*, 1991], modified to account for our coarser parameterization.

Inversion solutions were obtained by the damped least squares LSQR conjugate gradient method for sparse matrices [*Paige and Saunders*, 1982a b]. The travel time residuals for each ray are expressed as a function of velocities through each block multiplied by unknown velocity perturbations and summed along the ray path; the velocity in each block is assumed to be constant. The linear equations are $\mathbf{Ax=b}$, where the elements of matrix **A** are the coefficients arising from the summed velocity functions, the elements of **x** are the unknown velocity perturbations for which we solve, and the elements of **b** are the travel time residuals. After five iterations, the change in final RMS travel time fit values was insignificant. The largest decrease in RMS values took place after the first iteration (Figure 3a). Final RMS values were ~0.15 s, slightly larger than a typical measurement error, corresponding to a variance reduction of 50%. Damping was chosen that represented a balanced trade-off between smoothness of the model and fit to the data. We desired that the images be smooth enough to evaluate large structures but also that the travel time residuals not be overfit. Approximately 75% of the eigenvalues of normal matrix $\mathbf{A}^t\mathbf{A}$ were significant for our final trade-off choice of inversion parameters, supporting the parameterization scheme. This was determined by evaluating the eigenvalues (Figure 3b) and the log of each eigenvalue divided by the maximum eigenvalue (Figure 3c). This is an underdetermined problem, and many of the boxes in the grid space were not sampled by any rays.

3. Results

The resulting tomographic images show that heterogeneity is closely associated with tectonic features, in particular the Transverse Ranges and the San Andreas fault. Figure 4 shows the resulting velocity variations for the slice beneath the LARSE array (corresponding to slice 3 shown in Figure 1). The most prominent features are high *P* wave velocities (+6%) in the lower crust beneath the northernmost Los Angeles basin and the previously reported high-velocity anomaly beneath the San Gabriel Mountains and San Andreas fault (+3%). Several unique features stand out in the images. The upper mantle anomaly is narrow, it lies below the crustal root, and it extends up to the base of the crust without spreading laterally below the crust on either side of the mountains. The lack of spreading indicates that the presumably cold upper

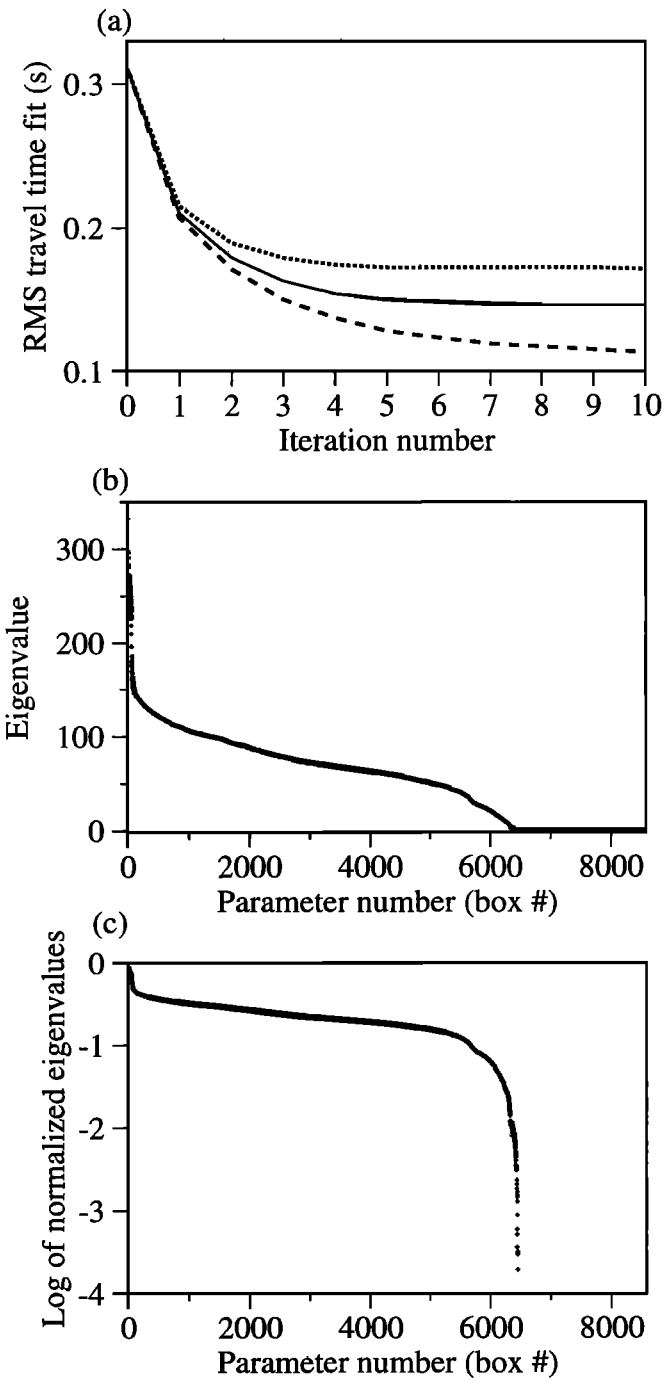

Figure 3. (a) Root-mean-square (RMS) travel time fit decrease with iteration number. Curves for several damping parameters are shown; the less damped systems show the smaller RMS values. (b) Eigenvalues of the $\mathbf{A}^t\mathbf{A}$ normal matrix and (c) the log of each eigenvalue divided by the maximum eigenvalue, arranged in decreasing order to show the number of significant eigenvalues, indicated by where the drop-off in the curves occurs.

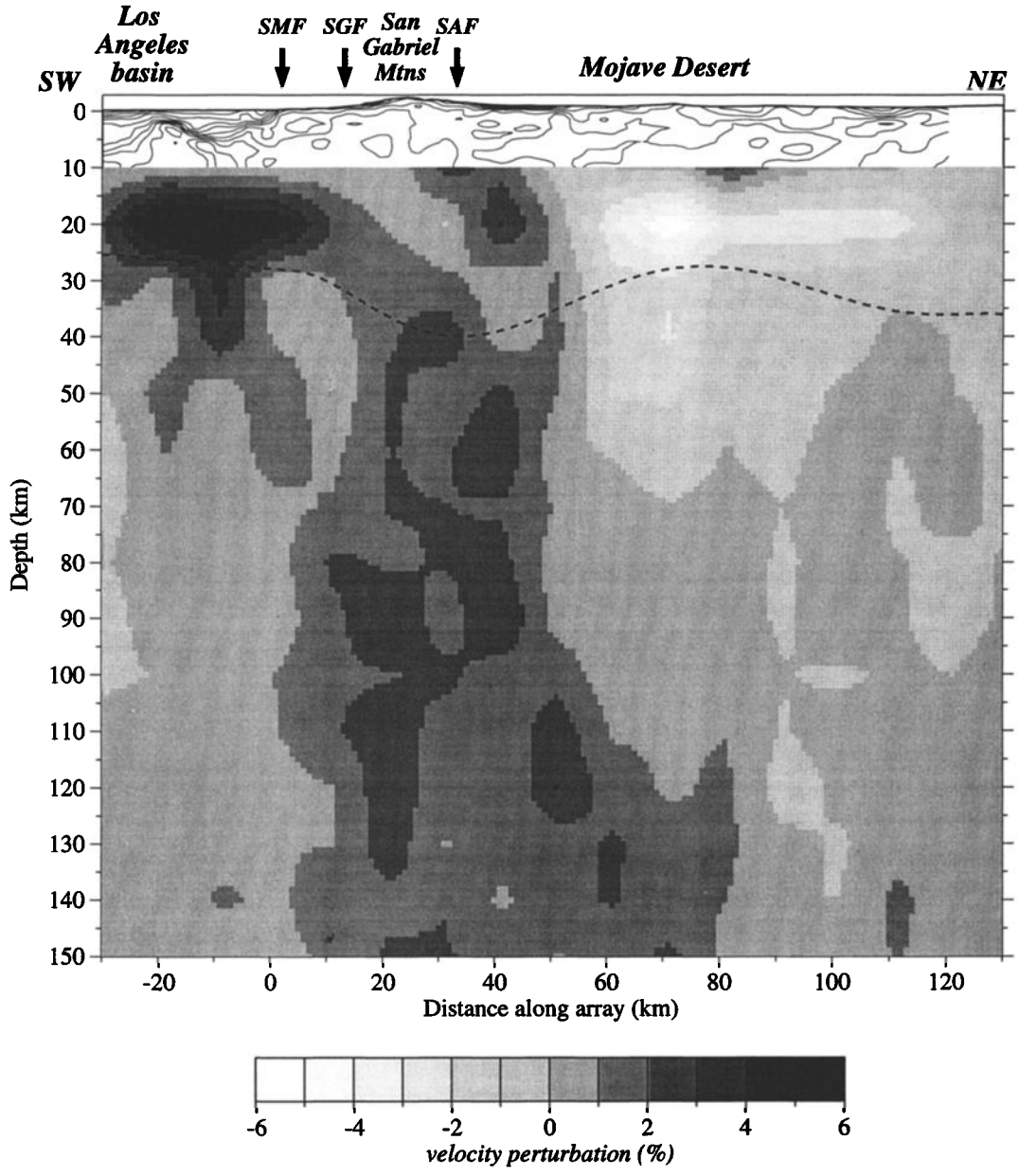

Figure 4. Velocity variations in cross-section slice beneath the LARSE array. The image has been smoothed by higher sampling and interpolation. The dashed curve is the Moho from *Kohler and Davis* [1997]. SMF, Sierra Madre fault; SGF, San Gabriel fault; and SAF, San Andreas fault.

mantle does not display the symmetric velocity profile that is predicted by one- or two-sided subductionlike downwelling [e.g., *Bird and Rosenstock*, 1984; *Humphreys and Hager*, 1990]. Relatively low velocities occur in the upper mantle below the Mojave Desert.

The high-velocity lower crust below the northernmost Los Angeles basin is clearly evident in the raw travel time data [*Kohler and Davis*, 1997]. The velocities suggest that the lowest 10 km of Los Angeles basin crust is composed of oceanic crust that extends to the southernmost San Gabriel Mountains, where it is replaced with continental crust. The high P wave velocity values correspond to lower crustal velocities of 6.9 km/s (relative to our starting velocity of 6.5 km/s). Alternatively, our high velocities may be due to significantly thinned crust beneath the basin, as proposed by *Kohler and Davis* [1997], if our assumed basin Moho depth of 25 km is an overestimate. Although ray path coverage is not as complete below the Los Angeles basin, vertical block resolution tests (discussed in section 4) show that this feature is most likely not an inversion artifact.

The upper 150 km of the upper mantle anomaly are shown in slices parallel to the LARSE array in Figure 5. The images illustrate that the anomaly is a localized feature that is not always deep. The anomaly width is similar to that of the overlying mountain ranges, and it is surrounded by average southern California lithospheric mantle velocities. The high velocities extend up to the base of the crust in each slice, although this structural feature is more poorly resolved than in

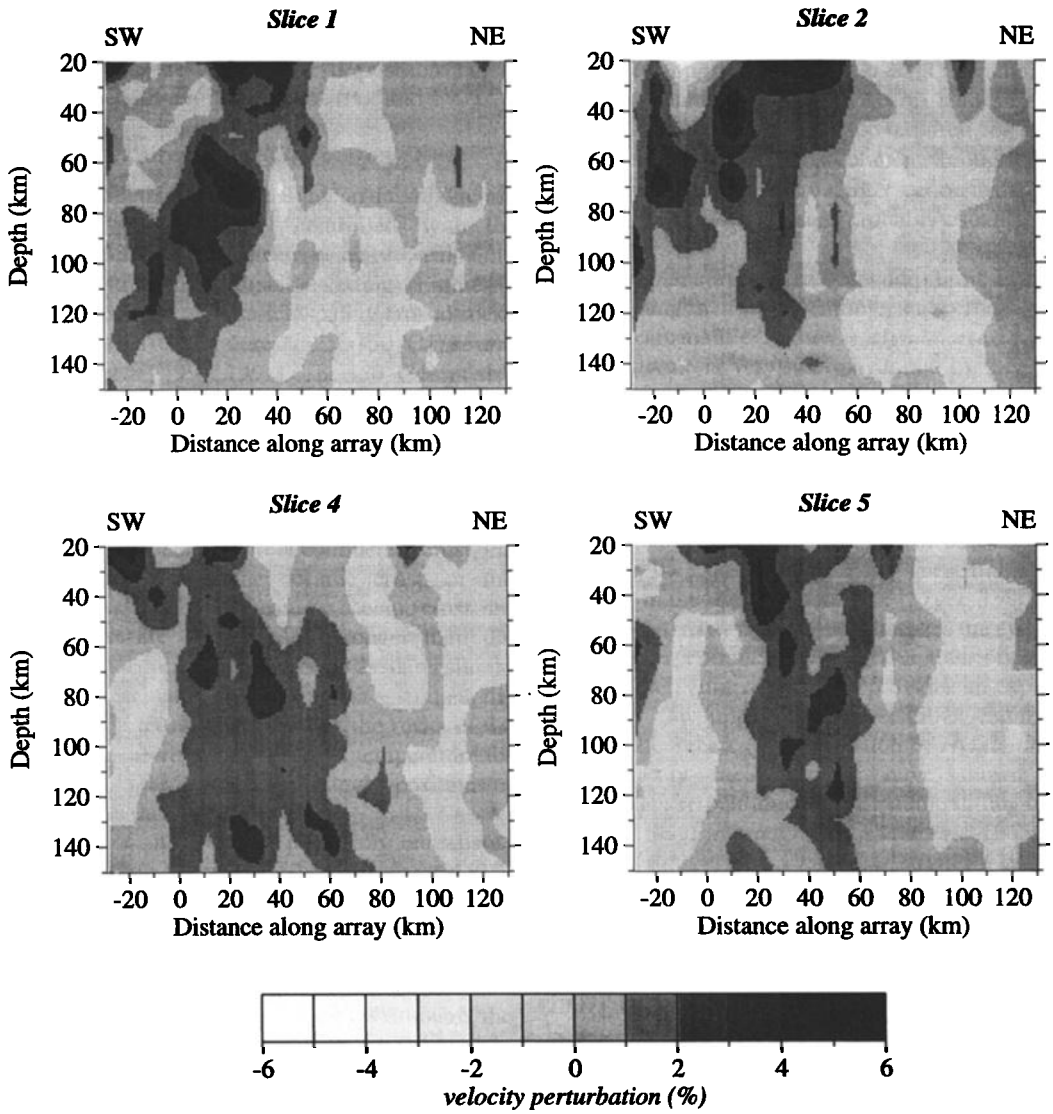

Figure 5. Velocity variations in cross-section slices parallel to array. See Figure 1 for locations corresponding to slice numbers.

Figure 5 because of the greater distance from the LARSE array. The anomaly is almost vertical in the center slice, but the deepest portion dips to the southwest in other slices. The images show lower than average, shallow lithospheric velocities beneath the Mojave Desert immediately adjacent to the Transverse Ranges.

Plan view images are shown in Figure 6 and illustrate how the anomaly width strongly correlates with geomorphological features associated with the plate boundary. At 30 km depth, it is approximately centered beneath the San Andreas fault (west side of the grid in Figure 6). At 60 km depth, it has rotated slightly, so that it is still centered on the San Andreas fault (middle of the grid in Figure 6) but shows an east-west trend. The east-west trend and correlation with surface features is less pronounced at depths >100 km. The diminishing amplitude with depths >100 km is most likely an inversion artifact related to ray path coverage.

The LARSE and SCSN data sets make complementary contributions to the final tomographic images. Since the LARSE-recorded rays approach the stations at incidence angles of 15°-30°, forming pyramidlike ray path coverage, they sample a depth interval of 20-40 km in each 20 km wide slice. The LARSE rays sample structure to a maximum depth of ~90 km in a slice of lithospheric structure that is up to 40 km away (horizontally) from the LARSE array (e.g., Figure 5). The LARSE data alone provide more detail within these narrow depth and distance intervals but do not add any information about deeper structures. The SCSN data alone allowed us to image coarser structure farther away from the LARSE array, structure in grid boxes not covered by LARSE ray paths, and deep features directly below the array.

4. Vertical and Lateral Resolution

Resolution tests indicate that the lateral resolution is good on a scale of 20 km and the vertical resolution is good for structures on a scale of 20-40 km, depending on ray path coverage. We determined resolution levels by inverting synthetic

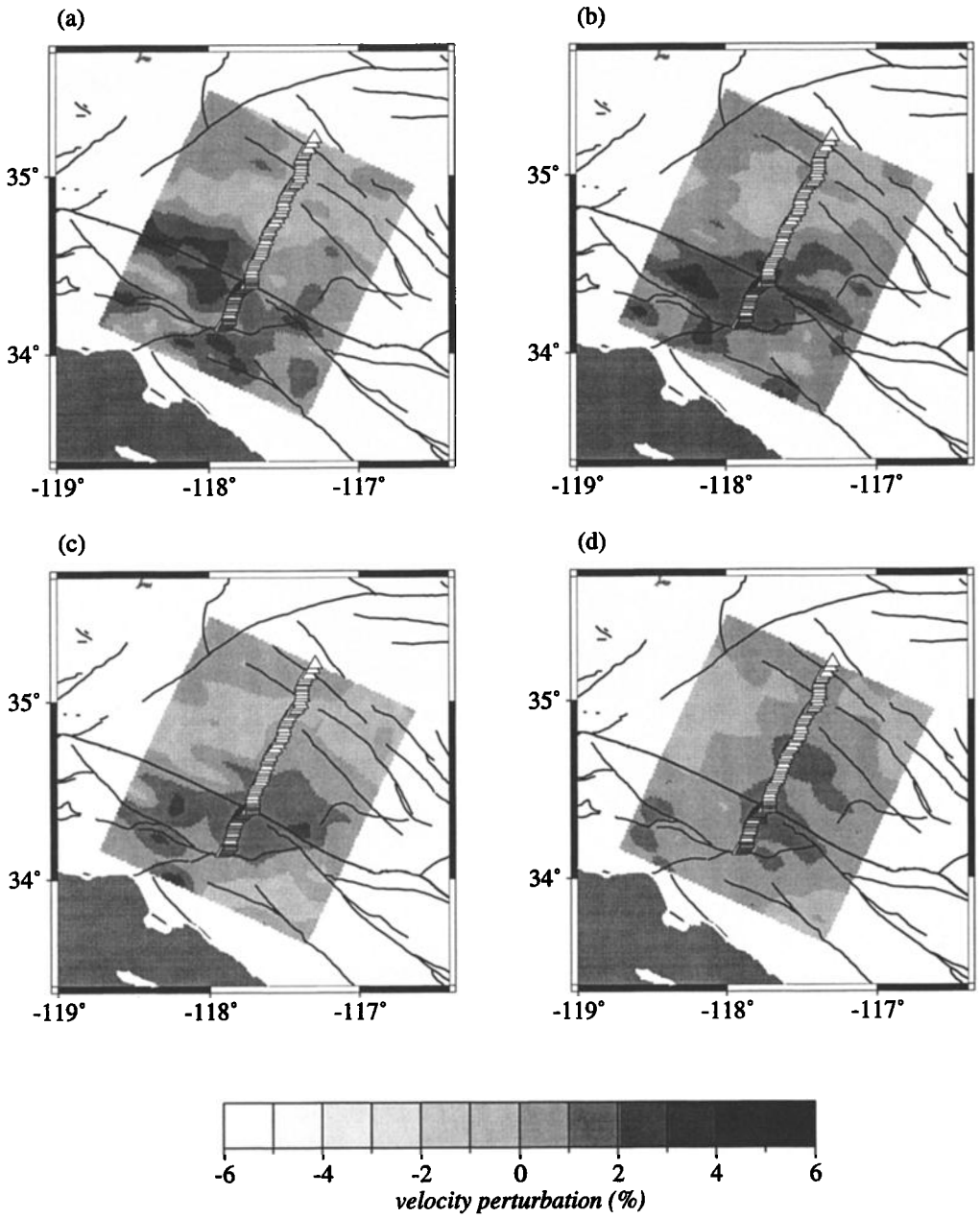

Figure 6. Plan views of velocity variations at depths of (a) 30 km, (b) 60 km, (c) 100 km, and (d) 150 km.

travel time residuals from forward modelling through synthetic Earth structure, in which one to several boxes are assigned a velocity perturbation. Two kinds of initial models were used: A checkerboard pattern test was used for lateral resolution, and vertical block pattern tests were used for depth resolution.

The checkerboard pattern resolution test supports the lateral location and width of the large-scale velocity anomalies shown in Figures 4-6. For this test, initial Earth structure was defined as alternating, 100 km deep, 20 km by 20 km vertical blocks of positive or negative velocity perturbation (either +6% or –6%). Rays were projected through the synthetic Earth models, and the resulting synthetic travel time residuals were inverted for Earth structure using the same inversion parameters as in the observed residual inversions. Initial patterns and results are shown in Figure 7 for depths of 30, 60, and 100 km. Recovered synthetic Earth structure is best for shallow depths (<60 km) in most of the grid space. Recovery is poor for deeper layers and for regions northeast and southeast of the array. Maximum recovered velocity amplitude is 80% relative to that of the initial Earth structure. The results of this resolution test help validate the observation that the upper mantle high-velocity anomaly is a narrow, sheetlike structure below thickened crust that includes the San Gabriel Mountains and San Andreas fault, and that it does not extend laterally to beneath the Los Angeles basin or the central Mojave Desert.

Vertical block pattern tests give us an indication of depth resolution for a column of high-velocity material beneath the San Gabriel Mountains. Rays were projected through syn-

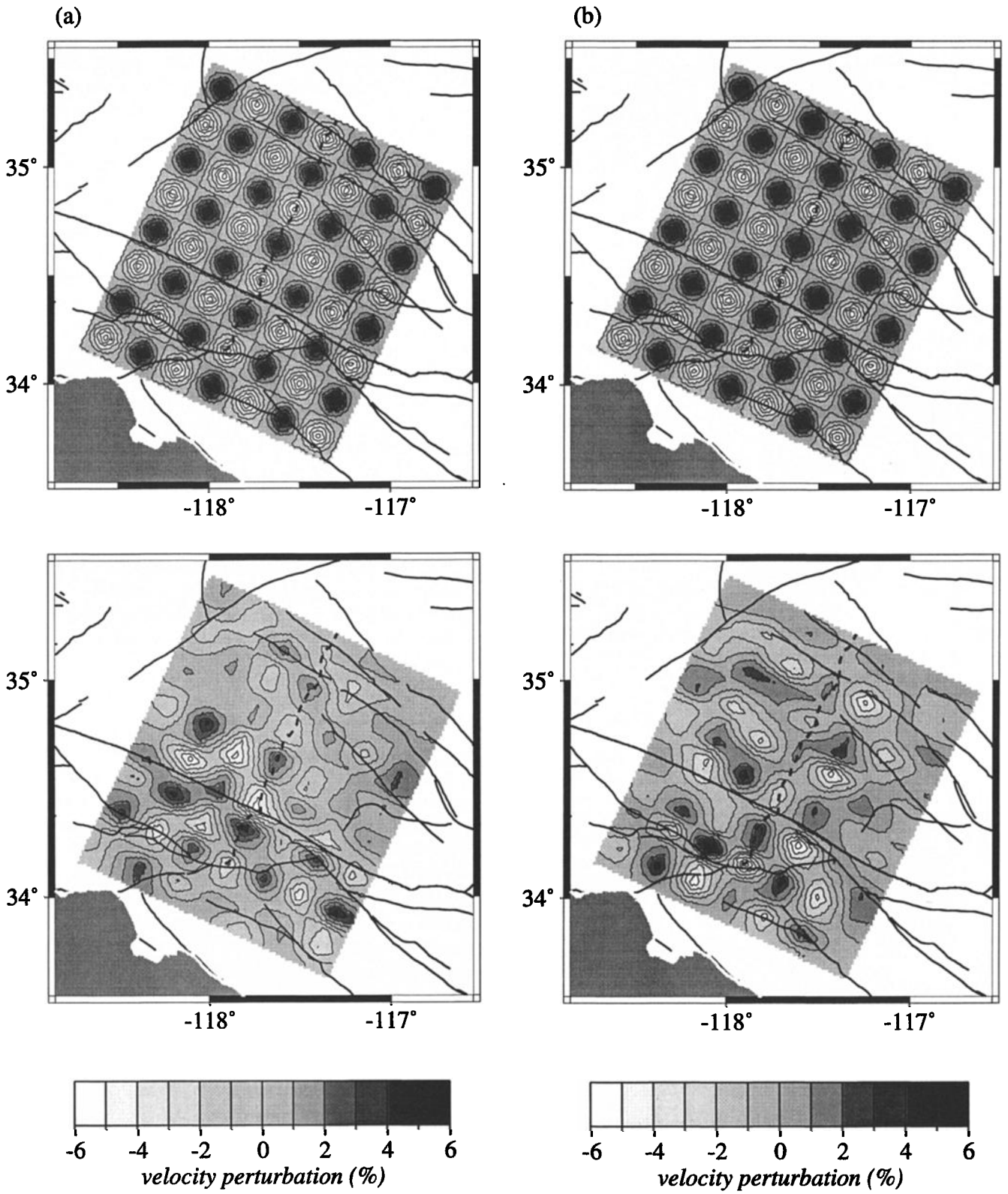

Figure 7. (top) Input and (bottom) resulting resolution patterns from checkerboard resolution test for depths of (a) 30 km, (b) 60 km, and (c) 100 km. Lateral resolution is best for shallow depths near the array where much of the original amplitude is recovered; less amplitude is recovered at greater depths.

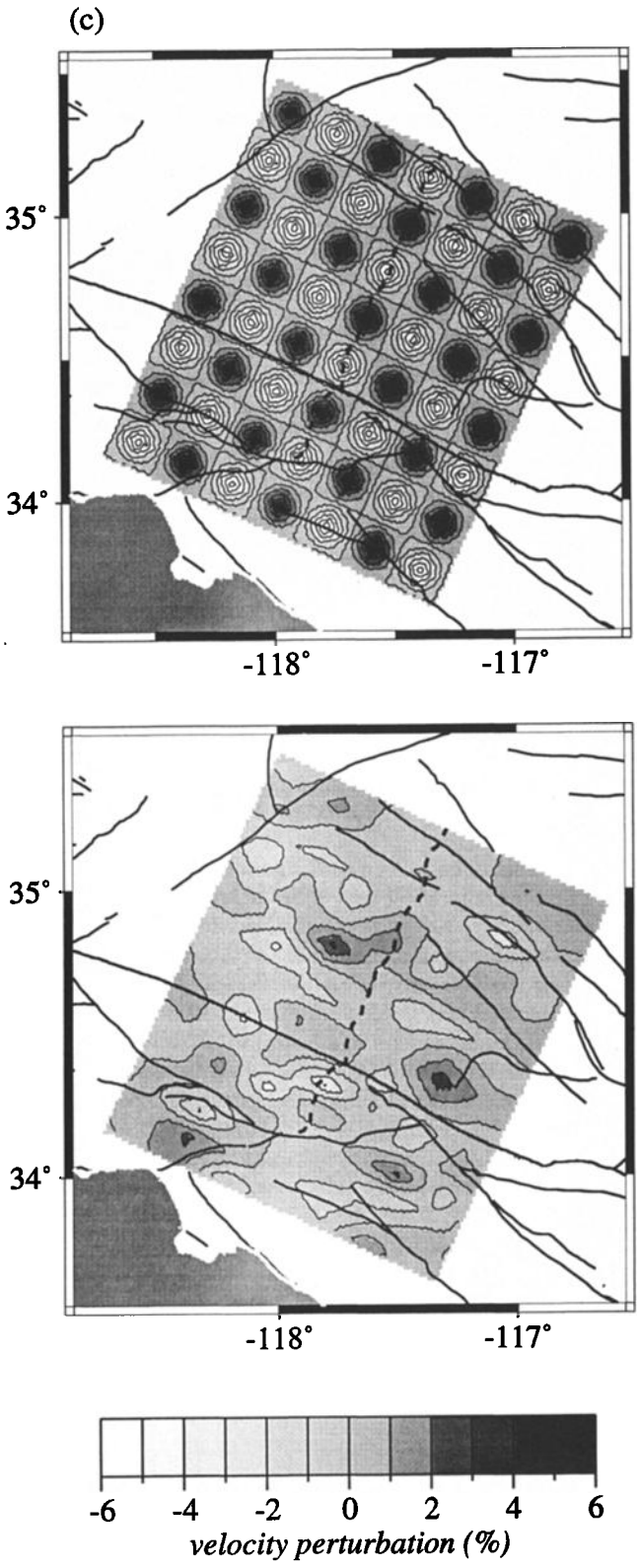

Figure 7. (continued)

thetic Earth models, and the resulting synthetic travel time residuals were inverted using the same inversion parameters as before. Input structures for the tests consisted of blocks below the San Gabriel Mountains with dimensions of 30 km parallel to the array by 20 km perpendicular to the array by 50 km deep (Figure 8a) and 30 km parallel to the array by 20 km perpendicular to the array by 110 km deep (Figure 8b). As Figure 8 shows, resulting lateral resolution is very good on this scale, and vertical resolution is best for depths less than ~100 km beneath the LARSE array. The synthetic structure tended to be displaced toward the surface, especially for longer blocks that were initially deeper; but the results of these tests demonstrate that we can still draw conclusions about the depths of large-scale features. The tests provide further support that the high-velocity anomaly lies directly below a region of thickened crust. The resolution tests also show, however, that the inversion may have placed the anomalous structures in regions too shallow by 20-40 km.

Similar vertical block pattern tests (Figure 9) provide validation that the high-velocity anomaly in the lower crust below the Los Angeles basin is a much smaller feature that is not part of a lithospheric-scale anomaly erroneously imaged in the lower crust. Input structures consisted of blocks below the Los Angeles basin with dimensions of 25 km parallel to the array by 20 km perpendicular to the array by 30 km deep (Figure 9a) and 25 km parallel to the array by 20 km perpendicular to the array by 50 km deep (Figure 9b). Although Figure 9 shows some vertical smearing, it suggests that the high-velocity anomaly is not an inversion artifact due to decreased ray path coverage. We cannot conclude from this test, however, that the high-velocity anomaly lies entirely in the lower crust and not in the uppermost 20-40 km of the mantle or vice versa. Computational constraints precluded us from performing the full, formal resolution analysis with the inverted normal matrix.

5. Discussion

The combination of network and array travel time data demonstrates the advantages of distinguishing small-scale seismic structures recorded in the dense array data from three-dimensional, large-scale heterogeneity seen in both array and network data. The tomographic images reported here differ from earlier studies primarily in the uppermost 90 km, where the LARSE data have revealed the geometry of structures not seen by larger networks alone. Our images show that the high-velocity anomaly in the upper mantle is a narrower, more localized feature than previously reported and that it extends up to the base of significantly thickened crust. This is in contrast to previous studies that have concluded that the crust is almost uniformly thick beneath the San Gabriel Mountains [*Hearn and Clayton*, 1986; *Sheffels and McNutt*, 1986; *Humphreys and Clayton*, 1990; *Sung and Jackson*, 1992] either by using independently determined crustal thickness estimates [*Hadley and Kanamori*, 1977; *Hearn*, 1984] or because they were not able to image smaller-scale kinematic features because of larger spatial sampling of travel times. The earlier crustal thickness models were only able to resolve features with dimensions greater than ~30 km because of the sparser data sets used, whereas *Kohler and Davis* [1997] were able to resolve the increase in crustal thickness that occurs over a horizontal distance of <20 km from the much denser LARSE array data. Consequently, the combined data inversions illus-

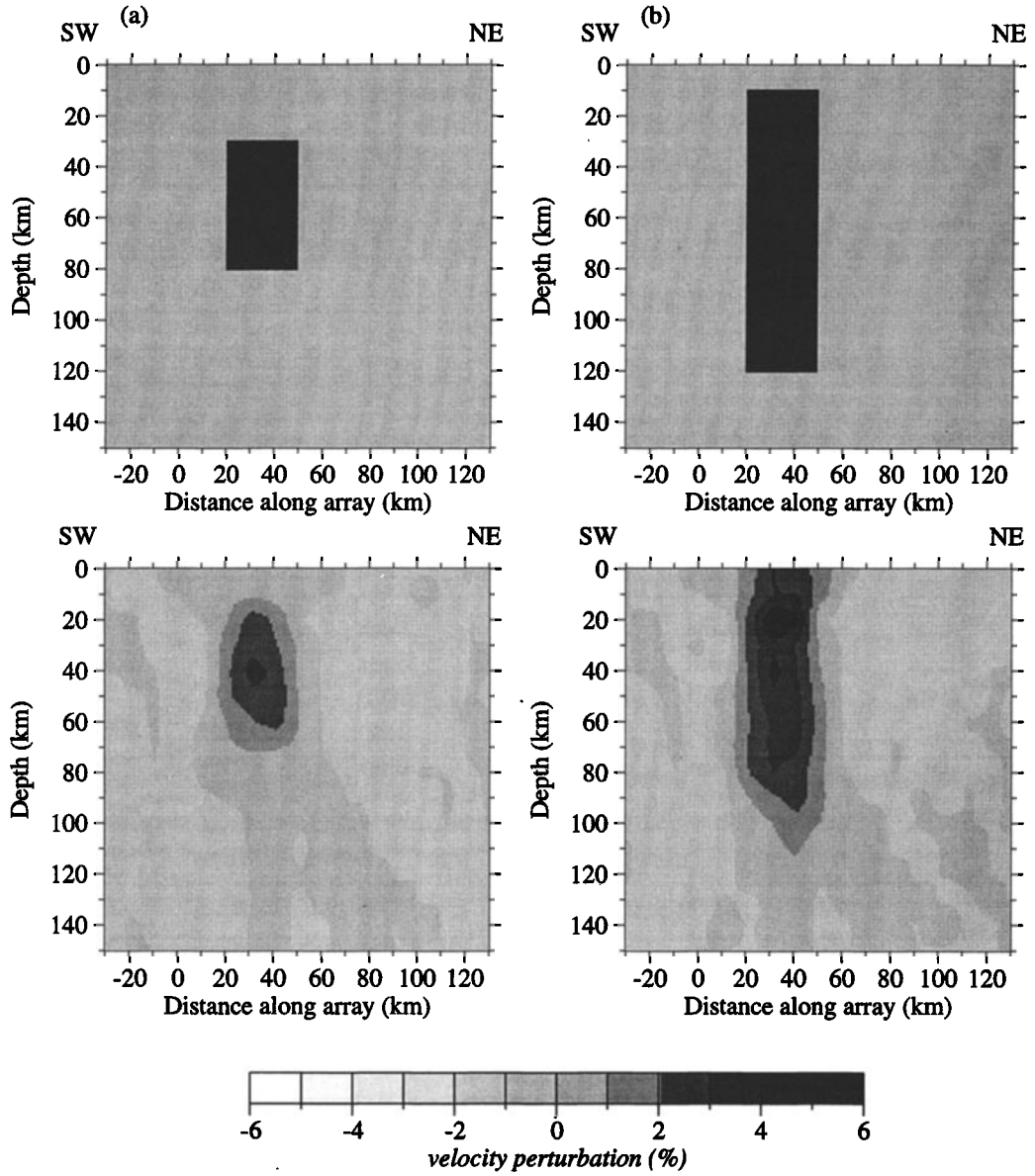

Figure 8. (top) Input and (bottom) resulting patterns from vertical block resolution tests for input blocks that are (a) 30 km parallel to the array by 20 km perpendicular to the array by 50 km deep and (b) 30 km parallel to the array by 20 km perpendicular to the array by 110 km deep. Note that lateral resolution is very good, vertical resolution is 20-40 km depending on the length of the block, but the block tends to be pushed up to the surface by the inversion.

trate how the thickened crust and anomalously fast upper mantle comprise a narrow, lithospheric-scale sheet of shortened, high-density material whose location may be associated with a convergent region centering on the plate boundary. Our results suggest that modeling of the tectonic evolution of the Transverse Ranges and of underlying mantle flow needs to take into account the observed crustal thickening and its kinematic relationship to upper mantle seismic anomalies.

5.1. Thermal and Density Structure

We argue that both the thickened crust and the high velocities in the uppermost mantle can be explained by uniform thickening of the entire lithosphere due to shortening under northeast-southwest compression. If we assume for the Transverse Ranges that the lower crust is mechanically coupled to some degree to the mantle lithosphere and that they have been thickened together, we can estimate the velocity heterogeneity expected from displacement of ductile lithosphere beneath the mountains relative to adjacent lithosphere below the basin and desert. In this scenario, simple downwarping of isotherms due to the mass displacement caused by the lithospheric shortening will produce lateral velocity and density variations in the mantle of the order of magnitude we observe. We make the conservative assumption for the uppermost mantle that the lithospheric isotherms beneath the San Gabriel Mountains are downwarped by an average of 20 km on the basis of crustal thickening estimates [*Hafner et al.*, 1996; *Kohler and Davis*, 1997; *Fuis*, 1998; *Ryberg and Fuis*,

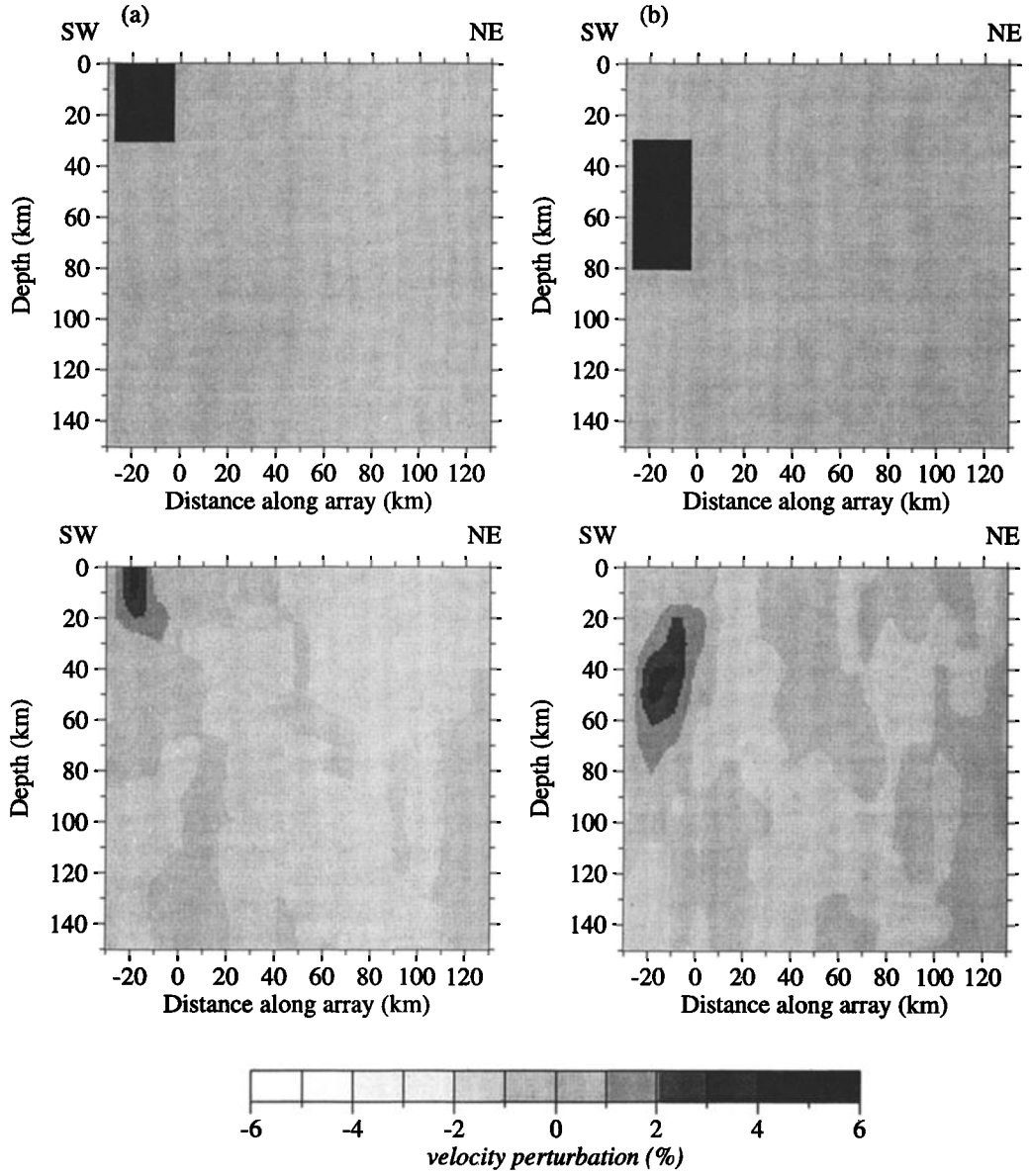

Figure 9. (top) Input and (bottom) resulting patterns from vertical block resolution tests for input blocks that are (a) 25 km parallel to the array by 20 km perpendicular to the array by 30 km deep and (b) 25 km parallel to the array by 20 km perpendicular to the array by 50 km deep. Note that lateral resolution is very good, but the block tends to be pushed up to the surface by the inversion.

1998]. In other words, colder material from above will be displaced to deeper locations. It may only be appropriate for the uppermost mantle, and we do not assume that the entire lithosphere has thickened by only 20 km. Changes in mantle temperature and density will affect the degree of downwarping with depth and time. Since convergence in the Transverse Ranges is a young (<6 Myr old), active process, the downwarped material has not had time to thermally equilibrate with undeformed material. We estimate the amount of lateral heterogeneity that will result from the displaced material, assuming that it is primarily due to temperature variations. Before compression and downwarping, two points A and B (Figure 10a) of upper mantle at the same depth are initially at the same temperature. Temperature as a function of depth in the shallow lithosphere ($\Delta T/\Delta z$) is approximately equal to 10°C/km assuming that heat is transported by conduction [*Turcotte and Schubert*, 1982; *Stacey*, 1992]. After shortening, two points in the upper mantle, A and B' (Figure 10b), at the same depth, are now at different temperatures from each other because B and B' have been displaced down 20 km, and mantle at point B' is cooler by ~200°C than mantle at point A. Laboratory experiments on mantle rocks indicate that the temperature derivative of compressional velocity ($\partial V_P/\partial T$) is approximately equal to -1.2×10^{-3} km/s/K at upper mantle pressures [*Sato et al.*, 1989]. This results in a +3% *P* wave velocity increase for a pocket of upper mantle material experiencing a 200°C temperature decrease relative to material elsewhere at the same depth and accounts for the values in the seismic images we obtained. This is likely an overly simple explanation for the

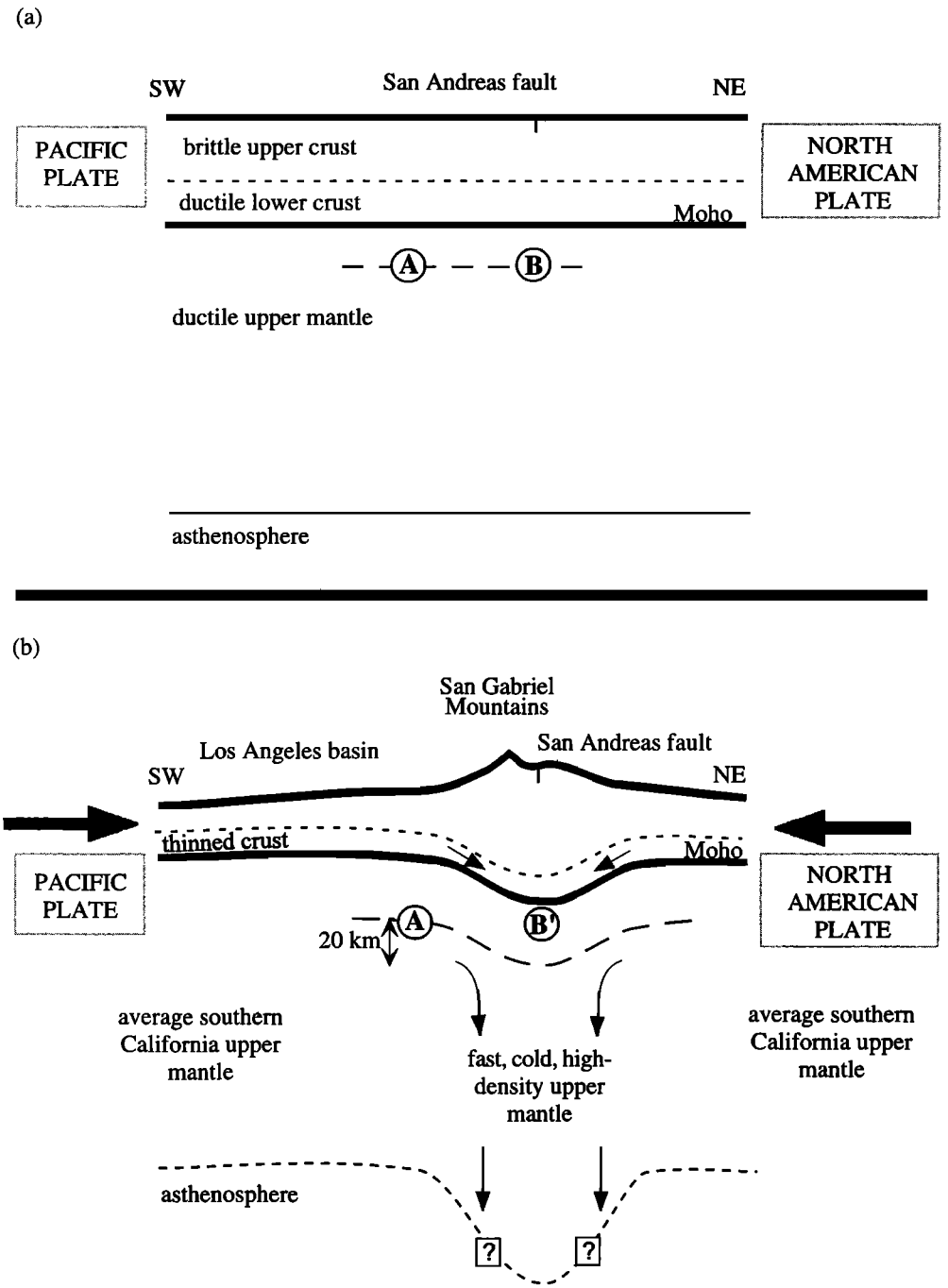

Figure 10. Schematic representation of kinematic model for lithospheric thickening and crust-mantle coupled deformation. (a) Isotherm structure in the lithosphere before deformation and downwarping. Points A and B are at the same depths and temperatures. (b) Isotherm structure after downwarping. Points A and B' are at the same depths but different temperatures because B' has been displaced down 20 km and is cooler than point A.

observed fast anomaly because the depth and temperature variations of density and viscosity will affect the depth extent of the isotherms, but it may explain the large-scale variations.

The correlation between features in our tomographic images and the geodetic measurements of fault-normal plate motion in the same region provides strong evidence that the crust and mantle lithosphere have thickened together in response to the last few million years of convergence. Recent plate motion estimates from geodetic observations in the left-step region of the San Andreas fault show that plate boundary convergence has resulted in crustal shortening accommodated by numerous blind thrust, strike-slip, and oblique-slip faults, many of which are at large distances from the San Andreas fault [*Feigl et al.*, 1993; *Shen et al.*, 1996, 1997; *Walls et al.*, 1998]. In a cross section close to our study area, *Shen et al.* [1996] obtain up to 15 mm/yr of total convergence normal to the San Andreas fault from GPS measurements. Geodetic studies also indicate that convergence is approximately cen-

tered on the San Andreas fault [*Shen et al.*, 1996; *Snay et al.*, 1996]. This suggests that some degree of mechanical and thermal coupling may have occurred as the crust and mantle lithosphere have been compressed. Deformation may have subsequently become partially or totally decoupled as higher-density upper mantle developed as a downwelling flow [e.g., *Humphreys and Hager*, 1990] away from the thickened crust.

Our observations and interpretation have new implications for upper crustal kinematics and dynamics. The independent rotations and translations observed in the crust [*Jackson and Molnar*, 1990; *Luyendyk*, 1991] and, in particular, the ongoing rotation of the Transverse Ranges block [e.g., *Nicholson et al.*, 1994] require a shear zone to accommodate their motion. Our interpretation favors a midcrustal shear zone, possibly associated with the brittle-ductile transition zone, to explain the present-day, predominantly horizontal motion. Independent evidence for a midcrustal detachment zone accommodated by a low-angle fault system is provided by seismic reflection modeling [*Ryberg and Fuis*, 1998] and is suggested by geodetic plate motion measurements [*Shen et al.*, 1996]. It would be difficult to explain the development of crustal or lithospheric thickness variations along a horizontal shear zone at the Moho or lithosphere-asthenosphere interface, respectively. Note that our crustal and mantle anomalies are centered on the San Andreas fault and not on the highest elevation of the San Gabriel Mountains. This suggests that ongoing plate boundary convergence and downwelling play a dominant role in the lower crustal and uppermost mantle kinematics and dynamics whereas motion along a midcrustal interface may control upper crustal deformation.

The small-scale seismic velocity gradients below the region of local maximum convergence are presumed to be accompanied by proportional density gradients. The increase in density can be calculated empirically as $\rho = -0.302a(m) + 0.302V_P$ where ρ is density, V_P is compressional velocity, and $a(m)$ is a function of the average molecular weight of mineral assemblages for different parts of the Earth [*Birch*, 1961]. Using values compiled by *Birch* [1961] corresponding to lithospheric rocks, a 3% increase in seismic velocities corresponds to a 2% increase in density. Thus mantle material in the high-velocity anomaly is at least 2% more dense than material elsewhere in normal-velocity lithosphere and may be gravitationally unstable.

5.2. Gravity and Mechanisms of Compensation

The lack of correlation between gravity and topography has led to the conclusion that the Transverse Ranges are regionally compensated by a stiff, elastic plate and do not have a substantial crustal root [*Sheffels and McNutt*, 1986], even though the Transverse Ranges appear to be in regional isostatic equilibrium [*Oliver*, 1980]. Although two-dimensional gravity measurements cannot uniquely constrain lithospheric structure, we show below that Bouguer anomaly data can be explained by a combination of several structures to illustrate that a simple correlation between a specific structure such as crustal or lithospheric root and gravity signature cannot be expected. We analyzed data from a detailed U.S. Geological Survey gravity survey consisting of >250 measurements taken along the same LARSE line and reduced to complete Bouguer anomalies using a crustal density of 2.67 g/cm^3 [*Langenheim and Jachens*, 1996].

To estimate the contribution of sediments and low-density upper crustal rocks to the gravity profile, we inferred their densities from the seismic refraction line upper crustal velocity model [*Lutter et al.*, 1999] using the Nafe-Drake velocity-density relationship [*Nafe and Drake*, 1957] and separated the layers into two-dimensional density contour polygons (Figure 11a). A density of 2.67 g/cm^3 was assumed for the rest of the crust. Theoretical gravity perturbations were calculated using the approach of *Talwani et al.* [1959] in order to compare with the measured gravity residuals. Individual theoretical curves were computed for the sediments and other low-density rocks, Moho depth variations [*Kohler and Davis*, 1997], upper mantle velocity perturbations (using a contour average of 1% density), and all structures combined, respectively. The result (Figure 11b) shows that the gravity residuals calculated for the deep Los Angeles basin sediments offset the gravity residuals because of thickened crust below the San Gabriel Mountains. The upper mantle high-density anomaly has a smaller but noticeable signature that also offsets the effect of the crustal root in the gravity profile.

The combination of crustal root and upper mantle heterogeneity suggests a more complex mechanism of isostatic compensation than simple Airy isostasy. The combined effects of thickened crust with upper mantle lateral velocity variations and presumed temperature and density gradients may contribute to the regional compensation of the Transverse Ranges. The crustal root may be developing in response to compressional forces and instability in the lithosphere rather than solely to support the crust.

6. Conclusions

High-resolution tomographic images from LARSE array and SCSN teleseismic data provide evidence that the crust and upper mantle below the San Gabriel Mountains and San Andreas fault in the Transverse Ranges have thickened in a 60-80 km wide, vertical sheet. The increase in tomographic image details can be attributed to the addition of the high-density LARSE array data to the more widely distributed SCSN data. *P* wave travel time inversions of the teleseismic data support the presence of the well-known upper mantle high-velocity anomaly that extends ~200 km into the mantle. Our three-dimensional images of upper mantle heterogeneity show that the high velocities are approximately centered on a large region of convergence that includes the Transverse Ranges and San Andreas fault but that the anomaly does not always extend vertically into the mantle. The images show that the anomaly lies below the base of a 10-12 km deep root because of lithospheric thickening in the crust and that there is no tomographic evidence for lateral extension of upper mantle high velocities on either side of the San Gabriel Mountains and southernmost Mojave Desert. The relationship between deformation geometry in the lower crust and upper mantle suggests that the deformation may be due to some degree of mechanical and thermal coupling and that it

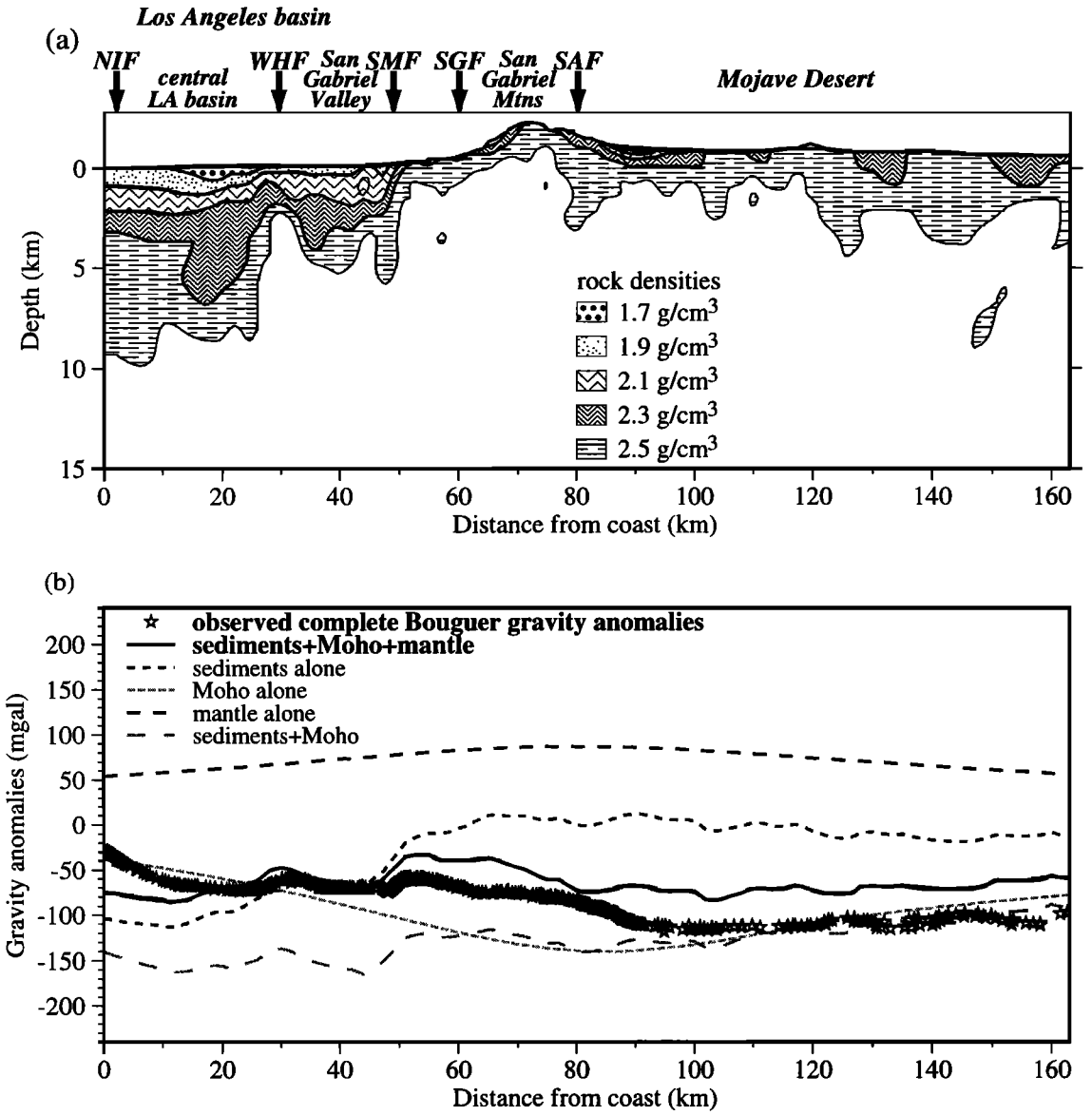

Figure 11. (a) Density contours inferred from seismic velocity contours of the *Lutter et al.* [1999] crustal model using the Nafe-Drake relationship [*Nafe and Drake*, 1957]. NIF, Newport-Inglewood fault; WHF, Whittier fault; SMF, Sierra Madre fault; SGF, San Gabriel fault; and SAF, San Andreas fault. (b) Theoretical two-dimensional gravity perturbations calculated using the *Talwani et al.* [1959] two-dimensional polygon approach for comparison with observed Bouguer gravity data.

may be caused by regional compression. Downwarping of the isotherms below the root due to lithospheric thickening would explain the 3% lateral *P* wave velocity variations. Bouguer gravity data are consistent with the existence of a crustal root and upper mantle high-density anomaly, suggesting that isostatic compensation involves both crust and uppermost mantle structural heterogeneity.

Acknowledgments. The work presented here was greatly strengthened by enlightening discussions with Paul M. Davis. The author wishes to thank Peter Bird, Ken Dueker, Rebecca Saltzer, the AE, and an anonymous referee in particular for valuable comments on the manuscript. LARSE was a joint effort involving scientists from the University of California at Los Angeles, the U.S. Geological Survey, the California Institute of Technology, and the University of Southern California. The LARSE experiment was made possible by the loan of IRIS PASSCAL seismometers and the support of its staff. Thanks go to Ken Dueker for providing the large compilation of Southern California Seismic Network *P* wave travel time residual data. Egill Hauksson and Bill Lutter were kind enough to forward their upper crustal velocity models. This research was supported by the Southern California Earthquake Center. SCEC is funded by NSF Cooperative Agreement EAR-8920136 and USGS Cooperative Agreements 14-08-0001-A0899 and 1434-HQ-97AG01718. The SCEC contribution number for this paper is 368.

References

Atwater, T., Implications of plate tectonics for the Cenozoic tectonic evolution of western North America, *Geol. Soc. Am. Bull., 81*, 3513-3536, 1970.

Birch, F., Composition of the Earth's mantle, *Geophys. J. R. Astron. Soc., 4*, 295-311, 1961.

Bird, P., and R. W. Rosenstock, Kinematics of present crust and mantle flow in southern California, *Geol. Soc. Am. Bull., 95*, 946-957, 1984.

Crowell, J. C., Movement histories of faults in the Transverse ranges and speculations on the tectonic history of California, in *Proceedings of the Conference on Geologic Problems of the San Andreas Fault System*, edited by W. R. Dickinson and A. Grantz, *Stanford Univ. Publ. Geol. Sci., 11*, 323-341, 1968.

Dokka, R. K., The Mojave extensional belt of southern California, *Tectonics, 8*, 363-390, 1989.

Engebretson, D. C., A. Cox, and R. G. Gordon, Relative motions between oceanic and continental plates in the Pacific basin, *Spec. Pap. Geol. Soc. Am. Spec. Pap. 206, 59*, 1985.

Feigl, K. L., et al., Space geodetic measurement of crustal deformation in central and southern California, 1984-1992, *J. Geophys. Res., 98*, 21,677-21,712, 1993.

Fuis, G. S., West margin of North America: A synthesis of recent seismic transects, *Tectonophysics, 288*, 265-292, 1998.

Hadley, D., and H. Kanamori, Seismic structure of the Transverse Ranges, California, *Geol. Soc. Am. Bull., 88*, 1469-1478, 1977.

Hafner, K., R. W. Clayton, and E. Hauksson, Mid and lower-crustal structure beneath the San Gabriel Mountains, CA (LARSE) (abstract), *Eos Trans. AGU, 77(46)*, Fall Meet. Suppl., F738, 1996.

Hauksson, E., and J. S. Haase, Three-dimensional V_P and V_P/V_S velocity models of the Los Angeles basin and central Transverse Ranges, California, *J. Geophys. Res., 102*, 5423-5453, 1997.

Hearn, T. M., *Pn* travel times in southern California, *J. Geophys. Res., 89*, 1843-1855, 1984.

Hearn, T. M., and R. W. Clayton, Lateral velocity variations in southern California, II, Results for the lower crust from *Pn* waves, *Bull. Seismol. Soc. Am., 76*, 511-520, 1986.

Humphreys, E. D., and R. W. Clayton, Tomographic image of the southern California mantle, *J. Geophys. Res., 95*, 19,725-19,746, 1990.

Humphreys, E. D., and K. G. Dueker, Western U.S. upper mantle structure, *J. Geophys. Res., 99*, 9615-9634, 1994.

Humphreys, E. D., and B. H. Hager, A kinematic model for the late Cenozoic development of southern California crust and upper mantle, *J. Geophys Res., 95*, 19,747-19,762, 1990.

Humphreys, E. D., and R. J. Weldon II, Deformation across the western United States: A local estimate of Pacific-North America transform deformation, *J. Geophys. Res., 99*, 19,975-20,010, 1994.

Humphreys, E. D., R. W. Clayton, and B. H. Hager, A tomographic image of mantle structure beneath southern California, *Geophys. Res. Lett., 11*, 625-627, 1984.

Jackson, J., and P. Molnar, Active faulting and block rotations in the western Transverse Ranges, California, *J. Geophys. Res., 95*, 22,073-22,087, 1990.

Kennett, B. L. N., and E. R. Engdahl, Traveltimes for global earthquake location and phase identification, *Geophys. J. Inter., 105*, 429-465, 1991.

Kohler, M. D., and P. M. Davis, Crustal thickness variations in southern California from Los Angeles Region Seismic Experiment passive phase teleseismic travel times, *Bull. Seismol. Soc. Am., 87*, 1330-1344, 1997.

Kohler, M. D., P. M. Davis, H. Liu, M. Benthien, S. Gao, G. S. Fuis, R. W. Clayton, D. Okaya, and J. Mori, Data report for the 1993 Los Angeles Region Seismic Experiment (LARSE93), southern California: A passive study from Seal Beach northeastward through the Mojave Desert, *U.S. Geol. Surv. Open File Rep., 96-85*, 82 pp., 1996.

Langenheim, V. E., and R. C. Jachens, Gravity data collected along the Los Angeles Regional Seismic Experiment (LARSE) and preliminary model of regional density variations in basement rocks, southern California, *U.S. Geol. Surv. Open File Rep., 96-682*, 25 pp., 1996.

Lutter, W. J., G. S. Fuis, C. H. Thurber, and J. Murphy, Tomographic images of the upper crust from the Los Angeles Basin to the Mojave Desert, California: Results from the Los Angeles Region Seismic Experiment, *J. Geophys. Res.*, in press, 1999.

Luyendyk, B. P., A model for Neogene crustal rotations, transtension, and transpression in southern California, *Geol. Soc. Am. Bull., 103*, 1528-1536, 1991.

Nafe, J. E., and C. L. Drake, Variations with depth in shallow and deep water marine sediments of porosity, density and the velocities of compressional and shear waves, *Geophysics, 22*, 523-552, 1957.

Nicholson, C., C. C. Sorlien, T. Atwater, J. C. Crowell, and B. P. Luyendyk, Microplate capture, rotation of the western Transverse Ranges, and initiation of the San Andreas transform as a low-angle fault system, *Geology, 22*, 491-495, 1994.

Oliver, H. W., Transverse Ranges, in *Interpretation of the Gravity Map of California and its Continental Margin*, edited by H. W. Oliver, *Bull. Calif. Div. Mines Geol. 205*, 15-17, 1980.

Paige, C. C., and M. A. Saunders, LSQR: An algorithm for sparse linear equations and sparse least squares, *Trans. Math Software, 8*, 43-71, 1982a.

Paige, C. C., and M. A. Saunders, Algorithm 582, LSQR: Sparse linear equations and least squares problems, *Trans. Math Software, 8*, 195-209, 1982b.

Raikes, S. A., Regional variations in upper mantle structure beneath southern California, *Geophys. J. R. Astron. Soc., 63*, 187-216, 1980.

Ryberg, T., and G. S. Fuis, The San Gabriel Mountains bright reflective zone: possible evidence of young mid-crustal thrust faulting in southern California, *Tectonophysics, 286*, 31-46, 1998.

Sato, H., I. S. Sacks, and T. Murase, The use of laboratory velocity data for estimating temperature and partial melt fraction in the low-velocity zone: Comparison with heat flow and electrical conductivity studies, *J. Geophys. Res., 94*, 5689-5704, 1989.

Sheffels, B., and M. McNutt, Role of subsurface loads and regional compensation in the isostatic balance of the Transverse Ranges, California: Evidence for intracontinental subduction, *J. Geophys. Res., 91*, 6419-6431, 1986.

Shen, Z., D. D. Jackson, and B. X. Ge, Crustal deformation across and beyond the Los Angeles basin from geodetic measurements, *J. Geophys. Res., 101*, 27,957-27,980, 1996.

Shen, Z., D. Dong, T. Herring, K. Hudnut, D. Jackson, R. King, S. McClusky, and L. Sung, Crustal deformation measured in southern California, *Eos Trans. AGU, 78(43)*, 477, 482, 1997.

Snay, R. A., M. W. Cline, C. R. Philipp, D. D. Jackson, Y. Feng, Z.-K. Shen, and M. Lisowski, Crustal velocity field near the big bend of California's San Andreas fault, *J. Geophys. Res., 101*, 3173-3185, 1996.

Stacey, F. D., *Physics of the Earth*, 513 pp., Brookfield Press, Brisbane, 1992.

Stock, J. M., and K. V. Hodges, Pre-Pliocene extension around the Gulf of California and the transfer of Baja California to the Pacific plate, *Tectonics, 8*, 99-115, 1989.

Sung, L.-Y., and D. D. Jackson, Crustal and uppermost mantle structure under southern California, *Bull. Seismol. Soc. Am., 82*, 934-961, 1992.

Talwani, M., J. L. Worzel, and M. Landisman, Rapid gravity computations for two-dimensional bodies with application to the Mendocino submarine fracture zone, *J. Geophys. Res., 64*, 49-59, 1959.

Tennyson, M. E., Pre-transform early Miocene extension in western California, *Geology, 17*, 792-796, 1989.

Turcotte, D. L., and G. Schubert, *Geodynamics: Applications of Continuum Physics to Geological Problems*, 450 pp., John Wiley, New York, 1982.

Walck, M. C., and J. B. Minster, Relative array analysis of upper mantle lateral velocity variations in southern California, *J. Geophys. Res., 87*, 1757-1772, 1982.

Walls, C., T. Rockwell, K. Mueller, Y. Bock, S. Williams, J. Pfanner, J. Dolan, and P. Fang, Escape tectonics in the Los Angeles metropolitan region and implications for seismic risk, *Nature, 394*, 356-360, 1998.

Wright, T. L., Structural geology and tectonic evolution of the Los Angeles basin, California, in *Active Margin Basins*, edited by K. T. Biddle, *AAPG Mem. 52*, 35-134, 1991.

Yeats, R. S., Neogene acceleration of subsidence rates in southern California, *Geology, 6*, 456-460, 1978.

Yerkes, R. F., T. H. McCulloh, J. E. Schoellhamer, and J. G. Vedder, Geology of the Los Angeles basin California: An introduction, *U.S. Geol. Surv. Prof. Pap. 420-A*, 1965.

Zhao, D., H. Kanamori, and E. Humphreys, Simultaneous inversion of local and teleseismic data for the crust and mantle structure of southern California, *Phys. Earth Planet. Inter., 93*, 191-214, 1996.

M. D. Kohler, Department of Earth and Space Sciences, University of California at Los Angeles, Los Angeles, California, 90095-1567.

(Received December 3, 1998; revised March 17, 1999; accepted March 31, 1999.)